Title page

Reduced fibrous capsule elastic fibers of biologic ECM-enveloped CIEDs in minipigs fitted with a compression mechanics model

Roche C. de Guzman [a,*], Allison Meer [a,b], Aidan Mathews [a,b], Atara Israel [a], Michael Moses [a], Clarence Sams [a], and Daniel Deegan [c]

[a] *Bioengineering Program, Department of Engineering, Hofstra University, Hempstead, New York, USA*

[b] *Department of Biology, Hofstra University, Hempstead, New York, USA*

[c] *Aziyo Biologics, Silver Spring, Maryland, USA*

[*] Corresponding author: Roche C. de Guzman, 133 Hofstra University, 203 Weed Hall, Hempstead, NY 11549, USA. Phone: +1 (516) 463-7058. E-mail: roche.c.deguzman@hofstra.edu.

Abstract

BACKGROUND: Fibrous capsules (Fb) in response to cardiovascular implantable electronic devices (CIEDs) including a pacemaker (P) system, can produce patient discomfort and difficulties in revision surgery due to their high compressive strength, potentially via elevated elastic fibers.

OBJECTIVE: To determine if biologic extracellular matrix-enveloped CIEDs (PECM) caused differential Fb properties.

METHODS: Retrieved Fb (-P and -PECM) from minipigs were subjected to biomechanical (shear oscillation and uniaxial compression) and histological (collagen I and elastin) analyzes.

RESULTS: Fb-PECM showed significant decreases compared to Fb-P at: low strain-loss modulus (390 vs. 541 Pa) across angular frequencies, high strain-compressive elastic modulus (1043 vs. 2042 kPa), and elastic fiber content (1.92 vs. 3.15 µg/mg tissue), particularly closer to the implant's surface (71% vs.

143% relative to skin dermis elastin) and verified with a solid mechanics hyperelasticity with direction-dependent fiber viscoelasticity compression simulation ($r^2 \geq 98.9\%$).

CONCLUSIONS: The biocompatible wrap composed of decellularized porcine ECM for CIEDs generated fibrous tissues with less elastic fibers which contributed to a more desirable material mechanics.

Keywords: Minipig study, cardiovascular implantable electronic devices, pacemaker, decellularized tissue ECM, foreign body reaction, fibrous tissue encapsulation, compression biomechanics, oscillation rheology, elastin and elastic fibers, 3D distribution, COMSOL Multiphysics hyperelastic simulation

1. Introduction

The formation of a fibrous capsule is a foreign body reaction (FBR) against nondegradable materials, long-term implanted into the host system, dependent on various factors including the material's physical and chemical surface properties [1-4]. This tough tissue is induced to wall-off and systemically-isolate foreign objects (like cardiovascular implantable electronic devices (CIEDs) with titanium housing and their polymer-coated leads) and is a general indicator for implant biocompatibility: the thinner the layer, the more compatible the material [3, 5, 6]. The fibrous capsule (also called fibrotic scar tissue or fibrosis) is mainly composed of compact collagen fibers, produced by activated fibroblasts, some, together with layers of loose granulation tissue, immune cells, blood vessels, and a variety of enzymes and signaling molecules [1, 7, 8]. Aside from collagen (mainly type I, with occasional types II and III) [9-11], fibrous capsules have other extracellular matrix (ECM) structures, most notably elastic fibers [1, 8, 12, 13]. Elastic fibers are responsible for elastic recoil after stretching and compression for reversible recovery after deformation caused by applied loads, particularly beneficial for the skin and blood vessels [14-16]. However, in fibrous capsules of medical implants, their presence may be detrimental. The major component (~ 90%) of these fibers is elastin. Initially, the relatively small (M_w ~ 60 kDa) soluble precursor tropoelastin is secreted by cells (such as fibroblasts), which then assemble and get crosslinked

(forming covalent bonds) to elastic fibers via elastogenesis. Lysyl oxidase (and related enzymes) oxidize lysine residues for crosslinking with other tropoelastins and ECM proteins including collagens.

The fibrous capsule FBR is dynamic (time-dependent) and constantly remodeled depending on the stimuli. CIEDs-induced fibrous tissues can be used to an advantage: to subcutaneously affix and prevent device migration [17-20]. Conversely, too much fibrosis causes unwanted scar appearance, local tissue hardness, high compressive strength, and difficulties during CIED generator changes and pacing lead revision surgeries. In patients with silicone breast implants, contracture, leading to increased stiffness, discomfort, and pain can be attributed to increased elastin expression [12, 15, 21]. Similarly, issues encountered with CIEDs may be due to the abundance of elastic fibers. Biological product (biologic) ECM envelopes from decellularized porcine small intestine submucosa (SIS) were developed [22-24] to potentially provide a subtle and balanced fibrous response. To investigate their underlying effect, this study compared fibrous capsule biomechanical and histological properties and associated elastic fiber distribution, from pacemakers without and with biologic ECM wrap in a short-term minipig subcutaneous model. A computer model was proposed and fitted to explain and verify the observed compressive stress-strain responses.

2. Materials and methods

2.1 Animals and fibrous dissection

Surgical procedures and animal care were conducted at an independent research organization (American Preclinical Services, Minneapolis, MN). Protocols were approved by the Institutional Animal Care and Use Committee (IACUC) and animals received humane care in compliance with "the Guide" [25]. Human pacemakers (pulse generators) with an attached, coiled pacing lead (Edora 8 SR-T and Solia JT 45, Biotronik, Lake Oswego, OR), without (P) and with (PECM) decellularized SIS ECM envelopes (CanGaroo® Envelope (medium), Aziyo Biologics, Silver Spring, MD) were implanted subcutaneously (at 8 per group) in contralateral ventral neck-chest of adult miniature pigs (minipigs), then sacrificed and

necropsied for a total of 3 months duration (based on [18]). Implants that failed before the endpoint were excluded from this study. After pacemaker retrieval (Fig. 1), the surrounding fibrous capsule (Fb) and adjacent adipose (Ad) with occasional underlying muscles were excised, trimmed, and assigned as groups (Fig. 2): **Fb-P** (fibrous from pacemaker only, n = 5) and **Fb-PECM** (fibrous from pacemaker in ECM, n = 2), with Ad (adipose, n = 4) control, where n = biological replicates (individual animals). Multiple technical replicates (≥ 3) were obtained per biological per testing to account for individual variability [26].

2.2 Shear oscillation rheology

Tissues were subjected to rotating shear oscillation at exponentially increasing angular frequencies (ω) per fixed maximum shear strain (γ) to obtain their viscoelastic properties: storage modulus (G'), loss modulus (G"), delta or shear stress to strain phase shift (δ) = $\tan^{-1}(\tan(\delta))$ in degrees from 0° (pure solids) to 90° (pure liquids), and dynamic modulus (magnitude of complex modulus ($G^* = G' + iG''$) = $|G^*|$ = $(G'^2 + G''^2)^{0.5} = G'/\cos(\delta)$. Cylindrical biopsies at 8 mm-diameter (d) (Fb inner down and outer surface up) were tested in DHR-2 (Discovery Hybrid 2, TA Instruments, New Castle, DE) using parallel plates with a probe d = 12 mm and gap assigned to 2 mm. Oscillation experiments were performed at 5% (low) and 40% (high) γ from 1-40 rad/s (0.16-6.34 Hz) ω.

2.3 Axial compression

Unconfined uniaxial compression was conducted to obtain [27]: true compressive stress (σ), strain (ε), and elastic modulus (E) = Δσ/Δε at 0-10% (low) and high 30-40% (high) ε. Samples with d = 8 mm and height (h) = entire Fb thickness were placed onto the baseplate (Fb inner down and outer surface up) and compressed with a 6 mm chamfered indenter at 0.1 mm/s until ~ 40-60% ε (Instron 3345, Norwood, MA). Instantaneous E = dσ/dε = numerical derivative of σ with respect to ε was reported (centered finite difference with a 2-term Taylor: $(d\sigma/d\varepsilon)_i = (-\sigma_{i+2} + 8\sigma_{i+1} - 8\sigma_{i-1} + \sigma_{i-2})/12(\varepsilon_i - \varepsilon_{i-1})$ [28]) to better display changes in $\sigma = f(\varepsilon)$.

2.4 Soluble elastin

Fastin™ elastin assay (Biocolor, Carrickfergus, Northern Ireland, UK) [29, 30] was employed to quantify elastic fibers (EFs) via released water-soluble α-elastin from tissues. Fresh specimens were processed through two rounds of α-elastin extraction (100 °C in 0.25 M oxalic acid), precipitation, and complexation with 5,10,15,20-tetraphenyl-21H,23H-porphine tetrasulfonate (TPPS). The complex was recovered, TPPS released, absorbance at 513-nm measured, converted to mass using standards, and normalized to tissue mass (compared to a pig skin control).

2.5 Tissue staining

Fb samples were processed for histology to determine microscopic thickness, morphology, and structure using Masson's trichrome [31] (MT, Trichrome Stain Kit ab150686, Abcam, Waltham, MA) [32] for connective tissue components (cell nuclei = purple, cytoskeleton = red, and tissue collagen = blue), Van Gieson's elastic (VGE, Elastic Stain Kit ab150667, Abcam) [33] for EFs = black strands, and immunohistochemistry (IHC) for detection (brown signals) of collagen type I (1:100 anti-human collagen I alpha-1 1200-1450 fragment (ab233080, Abcam) reacting to pig elastin [34]) and EF elastin (1:200 anti-pig, human, dog, chicken, rat, and cow mature elastin (ab21610, Abcam)) [30, 35, 36]. The 3D differential distribution of elastin was investigated using four 2D: one cross and three tangential (inner (in), middle (mid), and outer (out) surface) sections (Fig. 1).

Briefly, tissues were fixed in 10% neutral buffered formalin, stored in 70% ethanol (EtOH), trimmed, dehydrated in increasing EtOH then xylene, paraffin-embedded (Paraplast X-TRA®, Sigma-Aldrich, St. Louis, MO), sectioned (at 5-μm), placed on slides, and rehydrated. After staining with MT and VGE, samples were dehydrated and soaked in Histomount (Thermo Fisher Scientific, Waltham, MA). For IHC, rehydrated sections (1 negative (–) control and ≥ 1 experimental/slide) with dried boundaries were circled with a hydrophobic barrier (ImmunoPen, Sigma-Aldrich), endogenous peroxidase inhibited (0.3% H_2O_2), antigen retrieved (citrate pH 6 at 95 °C for 10 min), and blocked with 10% normal goat serum. Specimens were hybridized with 1° antibody (Ab) for 2 hr (while blocking buffer for (–)), processed with rabbit specific HRP/DAB (ABC) Detection IHC Kit (ab64261, Abcam) [37], and mounted in

ImmunoHistoMount (Sigma-Aldrich). Human skin (Sigma-Aldrich and Aziyo Biologics) (comparable to pig skin [38]) and ECM envelope (Aziyo Biologics) were included as controls.

Images were captured in Cytation 5 (Agilent, Santa Clara, CA) and processed with GIMP (gimp.org), PowerPoint (Microsoft, Redmond, WA), and ImageJ (NIH, Bethesda, MD). IHC area ratios were quantified in thresholded and leveled images using ImageJ's analyze particle area sum over polygonal tissue area selection. Individual slide (–) signals were subtracted.

2.6 Modeling of compression

COMSOL Multiphysics (COMSOL, Stockholm, Sweden) using the solid mechanics interface with nonlinear structural materials module was employed to generate a 3D time-dependent compression model matching the experimental using parameters: Fb (E = 295 kPa (determined through parametric sweep), density (ρ) = 1.05 g/mL, and Poisson's ratio (ν) = 0.4999) and EF properties (E = 400 kPa (calculated based on [39]) and ρ = 1.2 g/mL). Fb was assumed as neo-Hookean hyperelastic incompressible [40]. EFs were modeled with direction-dependent (tangential and axial) domain node fibers (linear elastic with a volume fraction or ratio (r_v)). The tissue was divided into sections (in, mid, and out) and each assigned with fibers with viscoelasticity of a single-branch generalized Maxwell containing: energy factor (f_e) and relaxation time (t_r) [39]. A rigid indenter at 0.1 mm/s prescribed velocity compressed Fb with constrained bottom boundary to 40%. Unstructured uniformly-distributed quadrilateral meshes along h was used. Average of the domain's top boundary in contact with the probe was evaluated for stress = Gauss point von Mises stress and strain = displacement/h.

2.7 Data analysis

Data were processed in Excel (Microsoft) and MATLAB (Mathworks, Natick, MA). Technical replicate values were averaged, and biological replicates' values again averaged then reported as mean ± standard deviation. Student's t-test and analysis of variance (ANOVA, 1 and 2-factor) with Tukey-Kramer were used for comparison using a probability (p) < 0.05 deemed significantly different and represented as: ***p < 0.001, **p < 0.01, and *p < 0.05.

3. Results

3.1 Fibrous capsule gross evaluation

Implants induced the expected Fb tissues [41] (Fig. 1) in the subcutaneous region. The fibrous appearance was prominent in 3/5 (60%) and 1/2 (50%) for Fb-P (samples 1-3) and Fb-PECM (2), respectively (Fig. 2). These tissues vary in thicknesses in situ from ~ 2-6 mm within each sample and across biological replicates. They were attached to adipose (Ad) tissues on their outer, while their inner surfaces (adjacent to implant) were smooth, slippery, and lined with interstitial fluid [18, 42]. Localized blood patches (subcutaneous hematoma) were observed on inner sides in 3/5 (60%) and 1/2 (50%) of Fb-P (samples 1, 3, and 5) and Fb-PECM (1), likely due to the surgical procedure [43]. No signs of swelling were noticed.

3.2 Response to periodic shear

Fb tissues subjected to 5% γ oscillation showed G' > G" (Fig. 3a), indicating a more solid elasticity with $\delta < 45°$ (Fig. 3c), generally independent of ω. Characteristic of hydrogels [44], G' and G" displayed parallel plots due to their undamaged structures (nondestructive condition). The deformation was small to remain in the linear viscoelastic region (where data deemed reliable). The |G*| (resultant of G' and G") for Fb (P vs. PECM) were similar ($p = 0.063$), but fibrous had lower (***$p < 0.001$) |G*| than adipose tissues (Fig. 3b); showing that these connective tissue types can easily be distinguished. Importantly at **low γ, Fb-PECM's G" was statistically lower (*$p = 0.029$) compared to Fb-P's** (Fig. 3a, Table 1).

At 40% γ, G' trended at < G" (Fig. 3a) and $\delta > 45°$ (49-67° spread), pointing at materials with dominant fluid-like and viscous properties (typical hydrogel rheology at increased strain [45]). The high γ led to stretching which probably released bound water molecules and influenced the elevated loss modulus. Pairwise G' and G" demonstrated similarities despite an apparent lower pattern for Fb-PECM.

3.3 Effect of compression

Macroscopic thicknesses (for strain calculation) using a caliper yielded 4.0 ± 1.1 for Fb-P and 3.3 ± 0.5 mm for Fb-PECM, but still statistically similar ($p = 0.59$).

Compression to high strains (some up to ~ 60%) led to reversible deformation within the elastic region even with nonlinearity of the σ-ε curves (visco- and hyperelasticity of most biological materials [40, 46, 47]). Ad had drastically lower σ and its derivative (dσ/dε) compared to both Fb's (Fig. 4a-b), which rendered to lower (***p < 0.001 at 0-10% and at least *p < 0.05 at 30-40% ε) compressive E (Fig. 4c).

It is remarkable that Ad and Fb-PECM's curves had generally similar semi-log shapes (with adipose just translated downwards), while Fb-P's exhibited a distinct pattern (Fig. 4a) and more noticeable in numerical differentiation (Fig. 4b blue curves). Quantitatively **at high ε (30-40% or higher), Fb-P had significantly greater (*p = 0.026) slope or stiffer E than Fb-PECM** (Fig. 4c, Table 1), suggesting the presence of increased structural materials suspected as elastic fibers (EFs) with dominant stiffness during high strain conditions.

The E values for Ad fell within the acquired spread from human adipose [48]. Moreover, high-strain E of Fb were well within the 1.6-5.7 MPa of silicone implant fibrous capsules compressed at ~ 30% [12], supporting that our tests were sound and accurate.

3.4 Amount of α-elastin

Fibrous tissues were detected to contain more (**p = 0.002 for Fb-P and *p = 0.011 for Fb-PECM) elastin compared to adipose (Fig. 5). Importantly, **Fb-P had statistically higher (*p = 0.036) tissue elastin than Fb-PECM** (Fig. 5b, Table 1), indicating that the observed biomechanics differences were influenced by elastic fibers. This assay was deemed reliable since the obtained ratio of elastin in skin was around the expected 3.5 μg/mg [29].

3.5 Histology analysis

Sections from both Fb groups showed collagen ECM secreted by activated fibroblasts, filling the entire thickness with interspersed blood vessels (Fig. 6). Fb-PECM stained their cell nuclei faint and ECM lighter even after several repeats, perhaps due to differences in chemistry. Additionally for Fb-PECM, there were no signs of the ECM envelope suggesting full degradation [49] or removal together with the pacemaker. No foreign body giant cell was noticed indicating the absence of chronic

inflammation. In some, adipose tissue can be seen in the mid to outer zones, which indirectly indicated fibrous formation originating from the implant's surface. Regions with hematoma demonstrated reddish coloration in MT with round nuclei and brownish in VGE, likely as macrophages and blood contents, found in the inner as expected [1, 7, 8].

Microscopic thicknesses (2.7 ± 1.1 for Fb-P, 2.2 ± 0.3 for Fb-PECM, and 2.3 ± 0.1 mm for skin) were statistically similar ($p = 0.89$). Interestingly, the overall morphology of fibrous capsules resemble the skin dermis (Fig. 6 VGE); possibly they have similar tissue genesis.

Elastic fibers (EFs) (also seen from other Fb studies [1, 8, 12, 13]) were detected as black strands, visually more in cross-sections of Fb-P, especially in regions closer to the inner surface (Fig. 6 VGE inset). Immunostaining confirmed **higher (*p = 0.011) differentially-expressed EF elastin in Fb-P vs. Fb-PECM** (Fig. 7, Table 1, 1.49 ± 0.12 and 0.98 ± 0.25 relative to skin dermis levels). In tangential cuts (Fig. 7a boxed), there seemed to be more elastin in Fb-P (and in dermis) vs. Fb-PECM at inner and mid zones. Statistically, **Fb-P > Fb-PECM (*p = 0.024) at mid-tangential** (Fig. 7b, Table 1). Fb sections showed various stages of elastogenesis, ranging from diffuse elastin staining to assembled EFs with different orientations. The biologic ECM implant displayed lower (*at least $p < 0.05$) background elastin compared to others.

Collagen type I dominates the Fb ECM [9-11] and expression among tissue groups: Fb-P and Fb-PECM, including ECM envelope and skin dermis controls were found to be statistically similar ($p = 0.81$) (Fig. 8). Its density was qualitatively more intense in bundles, observed in the dermis (Fig. 6, Fig. 8a). Conversely, collagen I in fibrous capsules does not appear bundled but as separate fibers, suggesting less organization and maturation. EFs seem to not colocalize with collagen I in Fb samples.

3.6 Computer simulation

Simulation with 6-fold axially-oriented fibers at the inner and mid-Fb (in + 1/3 mid) relative to 12% r_v of tangential whole-tissue fibers (with consistent EF properties) resulted in a compressive σ-ε curve that agreed well ($r^2 = 99.7\%$) compared to experimental Fb-P observation, including elevated von Mises stress seen across tissue equivalent to higher compressive strength (Fig. 9a). When these axial elastic fibers

were removed (at 0 fiber, Fig. 9b-c), the plot fitted nicely to Fb-PECM experimental (Fig. 9d, r^2 = 98.9%). Different iterations of domain material models were simulated (Fig. 9e) but ultimately the hyperelastic with regional viscoelastic direction-dependent fibers showed the best for modeling Fb-P and Fb-PECM which agreed with experimental trends relating compression (Fig. 4a, Fig. 9d) to differential elastic fiber expression (Fig. 5b, Fig. 6, Fig. 7) using the viscoelasticity parameters: f_e = 2% and t_r = 50 s.

4. Discussion

The fibrous capsule response in this study was influenced by host contact to implant surface materials: titanium housing of pulse generator, epoxy resin of connector receptacle, silicone rubber of sealing plug, silicone rubber and polyurethane cover of pacing lead, and decellularized porcine SIS ECM of the wrap [22, 50]. Macro and micro-histologic features of recovered and processed fibrous tissues, without or with the biologic ECM treatment, indicate acceptable local FBR biocompatibility; expectedly as CIEDs being widely recognized clinically [40]. Despite similarities in appearance, thickness, and collagen type I morphology and content, we found five properties with statistically less magnitudes from Fb-PECM samples, summarized in Table 1. Changes in biomechanics at specific strain conditions can be explained by the anisotropic [51] levels of tissue elastin – its mature functional form represents the load-bearing elastic fibers. Perhaps the implant-isolating fibrous reaction against CIEDs is dermis-like, with analogous collagen and elastin quantities (Fig. 5, Fig. 6, Fig. 8). Alternatively, surface shielding with the ECM product generated a reduced near-implant elastic fibers, thereby with modified mechanics.

In the proposed hyperelastic model with viscoelastic fibers (Fig. 9), Fb-PECM was set as the starting fibrous tissue baseline, assuming at the early timeline of Fb-P's development that ultimately produced more elastic fibers. For this domain baseline, the simulated compressive stress-strain curve agreed with experimental once elastic fiber orientation was assigned as force-orthogonal (tangential or radial) and its tissue volume fraction to 12%, within acceptable degree of variability to the observed 8.6% (in cross-section). Addition and successive increase of force-parallel (axial) fibers to 6 times greater in the inner 44% region then gave us the accurate Fb-P compression model. The fiber ratio ultimately plateaued to

around 7-fold maximum capacity, indicating peak resemblance to the dermal tissue. It is noted that fibers placed closer to the implant provided better simulation outcome with higher stress-strain influence than when in the mid and outer zones. Overall, evidences considering statistics, potential sources of error, visual, and modeling analyses suggest that more elastic fibers are found towards CIED's surface in Fb-P. This also resulted in higher loss modulus taken in the rheology experiment due to elastic fiber-dependent increased water absorption and tissue retention [15, 52].

5. Conclusions

CIEDs wrapped in the biologic ECM caused reduced elastic fibers in the fibrous capsule region closer to the implant, which led to a more subtle biomechanical response including lower compressive strength with some likeness to surrounding adipose tissue, highlighting the potential of this technique for improved CIED's clinical use. A long-term study with more biological replicates for investigating elastic fiber anisotropy and associated cells and structures will be conducted afterwards.

Conflict of interest

Partial funding was obtained through Aziyo Biologics research grant.

Acknowledgements

We thank our research group undergraduates: Mariana Cabral, Megan Forst, Jayda Lewis, Andrew Tarabokija, Henna Chaudhry, and Evan Carroll for their lab assistance and feedback, Dr. Michael Dores (Biology) for help and access to imaging resources, and Engineering department and Hofstra University staff, especially Lori Castoria, Lynne Espiritu, Liz Downey, and Dean Sina Rabbany for overall support.

References

[1] Klopfleisch R, Jung F. The pathology of the foreign body reaction against biomaterials. *J Biomed Mater Res A*. 2017;**105**(3):927-40.

[2] Socarras TO, Vasconcelos AC, Campos PP, Pereira NB, Souza JP, Andrade SP. Foreign body response to subcutaneous implants in diabetic rats. *PLoS One*. 2014;**9**(11):e110945.

[3] Chung L, Maestas DR, Jr., Housseau F, Elisseeff JH. Key players in the immune response to biomaterial scaffolds for regenerative medicine. *Advanced drug delivery reviews*. 2017;**114**:184-92.

[4] Veiseh O, Vegas AJ. Domesticating the foreign body response: Recent advances and applications. *Advanced drug delivery reviews*. 2019;**144**:148-61.

[5] Welch NG, Winkler DA, Thissen H. Antifibrotic strategies for medical devices. *Advanced drug delivery reviews*. 2020;**167**:109-20.

[6] Gardner AB, Lee SK, Woods EC, Acharya AP. Biomaterials-based modulation of the immune system. *Biomed Res Int*. 2013;**2013**:732182.

[7] Hernandez JL, Park J, Yao S, Blakney AK, Nguyen HV, Katz BH, et al. Effect of tissue microenvironment on fibrous capsule formation to biomaterial-coated implants. *Biomaterials*. 2021;**273**:120806.

[8] Wagner W, Elbert SS, Zhang G, Yaszemski M. Biomaterials science : an introduction to materials in medicine. 4. ed. San Diego: Academic press is an imprint of Elsevier; 2020. pages cm p.

[9] Yang YH, Ard MB, Halper JT, Barabino GA. Type I collagen-based fibrous capsule enhances integration of tissue-engineered cartilage with native articular cartilage. *Ann Biomed Eng*. 2014;**42**(4):716-26.

[10] Brodsky B, Ramshaw JA. Collagen organization in an oriented fibrous capsule. *Int J Biol Macromol*. 1994;**16**(1):27-30.

[11] Akilbekova D, Bratlie KM. Quantitative Characterization of Collagen in the Fibrotic Capsule Surrounding Implanted Polymeric Microparticles through Second Harmonic Generation Imaging. *PLoS One*. 2015;**10**(6):e0130386.

[12] Poh PSP, Schmauss V, McGovern JA, Schmauss D, Chhaya MP, Foehr P, et al. Non-linear optical microscopy and histological analysis of collagen, elastin and lysyl oxidase expression in breast capsular contracture. *Eur J Med Res*. 2018;**23**(1):30.

[13] Hiebl B, Hopperdietzel C, Hunigen H, Dietze K, Jung F, Niehues SM. Tissue reaction induced by implanted venous access ports in adult patients after infection of the implantation site. *Clin Hemorheol Microcirc*. 2014;**58**(1):107-13.

[14] Vindin H, Mithieux SM, Weiss AS. Elastin architecture. *Matrix Biol*. 2019;**84**:4-16.

[15] Mithieux SM, Weiss AS. Elastin. *Adv Protein Chem*. 2005;**70**:437-61.

[16] Baumann L, Bernstein EF, Weiss AS, Bates D, Humphrey S, Silberberg M, et al. Clinical Relevance of Elastin in the Structure and Function of Skin. *Aesthet Surg J Open Forum*. 2021;**3**(3):ojab019.

[17] Ursaru AM, Haba CM, Popescu SE, Crisu D, Petris AO, Tesloianu ND. A Rare Entity-Percutaneous Lead Extraction in a Very Late Onset Pacemaker Endocarditis: Case Report and Review of Literature. *Diagnostics (Basel)*. 2021;**11**(1).

[18] Robotti F, Sterner I, Bottan S, Monne Rodriguez JM, Pellegrini G, Schmidt T, et al. Microengineered biosynthesized cellulose as anti-fibrotic in vivo protection for cardiac implantable electronic devices. *Biomaterials*. 2020;**229**:119583.

[19] Esposito M, Kennergren C, Holmstrom N, Nilsson S, Eckerdal J, Thomsen P. Morphologic and immunohistochemical observations of tissues surrounding retrieved transvenous pacemaker leads. *Journal of biomedical materials research*. 2002;**63**(5):548-58.

[20] Mancini MC, Grubb BP. A technique for the prevention of automatic implantable cardioverter defibrillator generator migration. *Pacing Clin Electrophysiol*. 1990;**13**(7):946-7.

[21] Kuriyama E, Ochiai H, Inoue Y, Sakamoto Y, Yamamoto N, Utsumi T, et al. Characterization of the Capsule Surrounding Smooth and Textured Tissue Expanders and Correlation with Contracture. *Plast Reconstr Surg Glob Open*. 2017;**5**(7):e1403.

[22] CanGaroo Envelope: Aziyo Biologics; [Available from: https://www.aziyo.com/products/electrophysiology/cangaroo/.
[23] Xiang K, Catanzaro JN, Elayi C, Esquer Garrigos Z, Sohail MR. Antibiotic-Eluting Envelopes to Prevent Cardiac-Implantable Electronic Device Infection: Past, Present, and Future. *Cureus*. 2021;**13**(2):e13088.
[24] Nayak H, Beaser AD, Aziz ZA. Patient Profiles in the Utilization of the CanGaroo(R) Envelope. *Cureus*. 2021;**13**(1):e12702.
[25] National Research Council (U.S.). Committee for the Update of the Guide for the Care and Use of Laboratory Animals., Institute for Laboratory Animal Research (U.S.), National Academies Press (U.S.). Guide for the care and use of laboratory animals. Washington, D.C.: National Academies Press,; 2011. Available from: http://grants.nih.gov/grants/olaw/Guide-for-the-Care-and-use-of-laboratory-animals.pdf.
[26] Bell G. Replicates and repeats. *BMC Biol*. 2016;**14**:28.
[27] Golshan A, Curtis JA, Lianos V, Rabbany SY, de Guzman RC. Compressive strengths of PEG gels with glycerol and bioglass particles. *Journal of Materials Research*. 2019;**34**(8):1341-52.
[28] Chapra SC. Applied numerical methods with MATLAB for engineers and scientists. Fourth edition. ed. New York, NY: McGraw-Hill Education; 2018. xvi, 697 pages p.
[29] Biocolor. Fastin Elastin Assay. 2015. p. 17.
[30] Halabi CM, Mecham RP. Elastin purification and solubilization. *Methods Cell Biol*. 2018;**143**:207-22.
[31] de Guzman RC, Merrill MR, Richter JR, Hamzi RI, Greengauz-Roberts OK, Van Dyke ME. Mechanical and biological properties of keratose biomaterials. *Biomaterials*. 2011;**32**(32):8205-17.
[32] ab150686 Trichrome Stain (Connective Tissue Stain): Abcam; [updated 18 September 2020. Version 3d:[Available from: https://www.abcam.com/ps/products/150/ab150686/documents/Trichrome-Stain-Kit-protocol-book-v3d-ab150686%20(website).pdf.
[33] ab150667 Elastic (Connective Tissue Stain): Abcam; [updated 14 August 2020. Version 3e:[Available from: https://www.abcam.com/ps/products/150/ab150667/documents/Elastic-Staining-protocol-book-v3e-ab150667%20(website).pdf.
[34] Anti-Collagen I antibody ab233080: Abcam; [Available from: https://www.abcam.com/collagen-i-antibody-ab233080.pdf.
[35] Mansfield J, Yu J, Attenburrow D, Moger J, Tirlapur U, Urban J, et al. The elastin network: its relationship with collagen and cells in articular cartilage as visualized by multiphoton microscopy. *Journal of anatomy*. 2009;**215**(6):682-91.
[36] Merrilees MJ, Ching PS, Beaumont B, Hinek A, Wight TN, Black PN. Changes in elastin, elastin binding protein and versican in alveoli in chronic obstructive pulmonary disease. *Respir Res*. 2008;**9**:41.
[37] Rabbit specific HRP/DAB (ABC) Detection IHC Kit ab64261: Abcam; [Available from: https://www.abcam.com/rabbit-specific-hrpdab-abc-detection-ihc-kit-ab64261.pdf.
[38] Rosenberg LK, Bagger C, Janfelt C, Haedersdal M, Olesen UH, Lerche CM. A Comparison of Human and Porcine Skin in Laser-Assisted Drug Delivery of Chemotherapeutics. *Lasers Surg Med*. 2021;**53**(1):162-70.
[39] Matsumoto T, Sugita S, Nagayama K. Tensile Properties of Smooth Muscle Cells, Elastin, and Collagen Fibers. In: Tanishita K, Yamamoto K, editors. Vascular Engineering: New Prospects of Vascular Medicine and Biology with a Multidiscipline Approach. Tokyo: Springer Japan; 2016. p. 127-40.
[40] Wex C, Arndt S, Stoll A, Bruns C, Kupriyanova Y. Isotropic incompressible hyperelastic models for modelling the mechanical behaviour of biological tissues: a review. *Biomed Tech (Berl)*. 2015;**60**(6):577-92.

[41] Imber G, Schwager RG, Guthrie RH, Jr., Gray GF. Fibrous capsule formation after subcutaneous implanation of synthetic materials in experimental animals. *Plastic and reconstructive surgery*. 1974;**54**(2):183-6.
[42] Cenaj O, Allison DHR, Imam R, Zeck B, Drohan LM, Chiriboga L, et al. Evidence for continuity of interstitial spaces across tissue and organ boundaries in humans. *Commun Biol*. 2021;**4**(1):436.
[43] Kumanomido J, Ohe M, Shibata R, Hattori Y, Ishizaki Y, Ito S, et al. Effective Use of Keishibukuryogan in Subcutaneous Hematoma after Implantable Cardiac Device Surgery in Two Cases. *Intern Med*. 2021;**60**(5):755-9.
[44] Franck A. Viscoelasticity and dynamic mechanical testing: TA Instruments; [updated 2017. Available from: https://www.tainstruments.com/pdf/literature/AAN004_Viscoelasticity_and_DMA.pdf.
[45] Pfaff NM, Dijksman JA, Kemperman AJB, van Loosdrecht MCM, Kleijn JM. Rheological characterisation of alginate-like exopolymer gels crosslinked with calcium. *Water Res*. 2021;**207**:117835.
[46] Gultekin O, Rodoplu B, Dal H. A quasi-incompressible and quasi-inextensible finite element analysis of fibrous soft biological tissues. *Biomech Model Mechanobiol*. 2020;**19**(6):2357-73.
[47] Sun Z, Lee SH, Gepner BD, Rigby J, Hallman JJ, Kerrigan JR. Comparison of porcine and human adipose tissue loading responses under dynamic compression and shear: A pilot study. *Journal of the mechanical behavior of biomedical materials*. 2021;**113**:104112.
[48] Alkhouli N, Mansfield J, Green E, Bell J, Knight B, Liversedge N, et al. The mechanical properties of human adipose tissues and their relationships to the structure and composition of the extracellular matrix. *Am J Physiol Endocrinol Metab*. 2013;**305**(12):E1427-35.
[49] Shi L, Ronfard V. Biochemical and biomechanical characterization of porcine small intestinal submucosa (SIS): a mini review. *Int J Burns Trauma*. 2013;**3**(4):173-9.
[50] Bradycardia Therapy: Biotronik; [Available from: https://www.biotronik.com/en-us/products/crm/bradycardia.
[51] Yu X, Wang Y, Zhang Y. Transmural variation in elastin fiber orientation distribution in the arterial wall. *Journal of the mechanical behavior of biomedical materials*. 2018;**77**:745-53.
[52] Wang Y, Hahn J, Zhang Y. Mechanical Properties of Arterial Elastin With Water Loss. *Journal of biomechanical engineering*. 2018;**140**(4).

Table

Table 1. Fibrous (Fb) tissue properties with significant difference.

Material Property		Fb-P	Fb-PECM	p
G" [Pa], at low-γ shear oscillation		390 ± 40	541 ± 54	*0.029
E [kPa], at high-ε compression		2042 ± 442	1043 ± 507	*0.026
released α-elastin from tissue [μg/mg]		3.15 ± 0.90	1.92 ± 0.33	*0.036
elastin in tissue section [%]:	cross	13.2 ± 1.1	8.6 ± 2.2	*0.011
	mid-tangential	12.6 ± 2.2	6.2 ± 1.6	*0.024

Figure Captions

Fig. 1. A pacemaker model (top left) implanted in the subcutaneous adipose (bottom left) with the subsequent fibrous capsule (Fb) response (bottom center). After retrieval (bottom right), select Fb with distinct inner and outer surfaces was cut into cross and tangential (in, mid, and out) sections (top right).

Fig. 2. Images of Fb-P (fibrous from pacemaker only, n = 5), Fb-PECM (fibrous from pacemaker in ECM, n = 2), and Ad (adipose control) surrounding tissues. Fibrous tissues are located inside the dashed outlines for both sample 1s. *Fb-P samples: 1-3 and Fb-PECM: 2 with pronounced fibrous connective tissue appearance. #Fb-P: 1, 3, and 5, and Fb-PECM: 1 had some regions of hematoma.

Fig. 3. a) Storage (G') and loss (G") moduli vs. angular frequency (ω) in a log-log plot at 5% and 40% maximum shear strain (γ) of Fb-P (blue) and Fb-PECM (green). G", 5% γ: Fb-P > Fb-PECM (*$p < 0.05$). b) Log-log (5% γ) of dynamic modulus (|G*|) vs. ω. Ad > Fb (***$p < 0.001$) c) Phase shift (δ) bar at 5% γ and 1, 10, and 40 rad/s ω.

Fig. 4. a) True compressive stress (σ) vs. strain (ε) in semi-log of Fb-P, Fb-PECM, and Ad technical replicates. Ad trended < Fb. Fb-P's curvature looks different compared to Fb-PECM and Ad's, highlighted in the next graph. b) Semi-log of instantaneous elastic modulus ($d\sigma/d\varepsilon$) vs. ε, indicating 0-10% (gray) and 30-40% (black double arrows) regions. c) Compressive elastic modulus (E) at 0-10%

(top) and 30-40% (bottom) ε. Pairwise significance: *p < 0.05 and ***p < 0.001, notably: Fb-P > Fb-PECM at 30-40% ε.

Fig. 5. a) Reddish-brown TPPS after release from α-elastin pellet. b) Normalized elastin-to-tissue mass ratio of Fb and Ad with a skin control. Pairwise significance: *p < 0.05 and **p < 0.01, importantly: Fb-P > Fb-PECM.

Fig. 6. Connective tissue stains: Masson's trichrome (MT) and Van Gieson's (VGE) of representative Fb cross-sections with layers spanning from the implant-adjacent inner to the outer surface attached to Ad. Human skin VGE with epidermis and dermis tissues included. Boxed insets demonstrate magnified regions with fibroblasts, collagen ECM (blue in MT), and elastic fibers (black strands in VGE).

Fig. 7. a) Representative elastin-IHC sections with negatives (–) from Fb and biologic ECM and skin (showing epidermis and dermis tissues) controls. Visually, Fb-P > Fb-PECM for in and mid tangential and cross-sections. b) Elastin in tissue area ratio compared to dermis bar graph. Mid-tangential and cross-sections: Fb-P > Fb-PECM (*p < 0.05). ECM < others (*p < 0.05).

Fig. 8. a) Collagen I-IHC cross-sections from Fb, ECM, and skin dermis. b) Bar of collagen I in tissue area ratio with 47-55% range.

Fig. 9. a) Graphical 3D of von Mises stress and deformation of Fb compression simulation at 40% ε. b) Compressive stress (σ) vs. axial fiber amount, indicating 0 for Fb-PECM and 6 for Fb-P. c) Locations and directions of fibers in Fb domains. d) Nonlinear scatterplot of σ vs. ε, displaying good agreement between Fb experimental (Exp) and simulation (Sim) values. e) σ vs. ε Sim curves of various material models.

Figures

Fig. 1

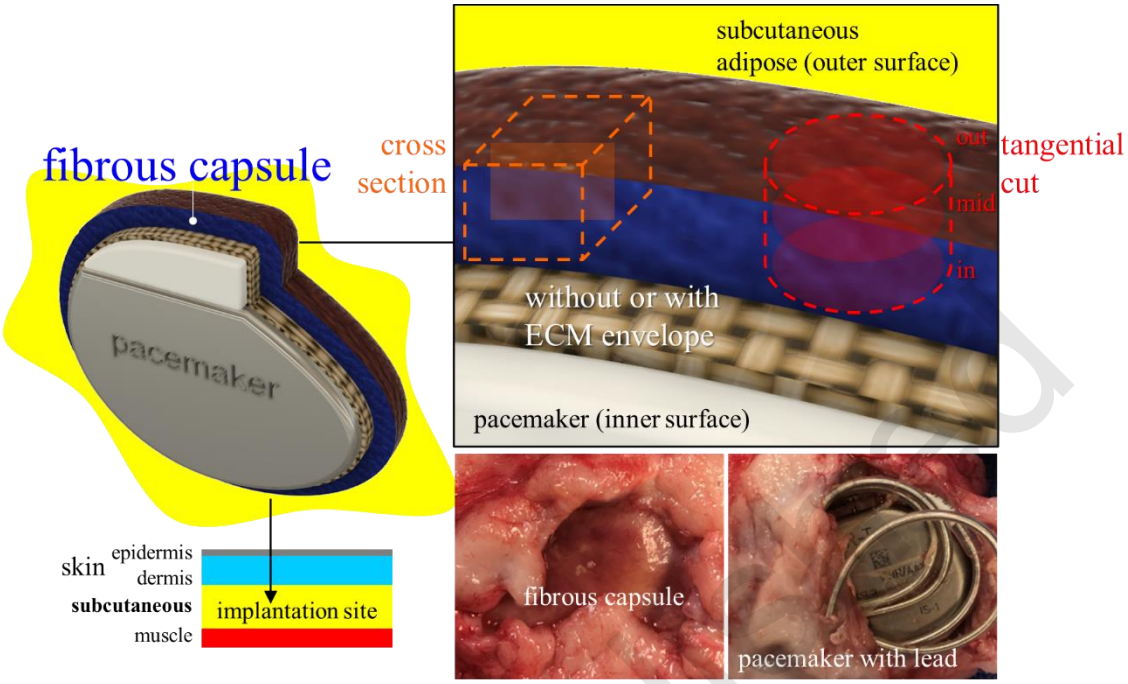

Fig. 2

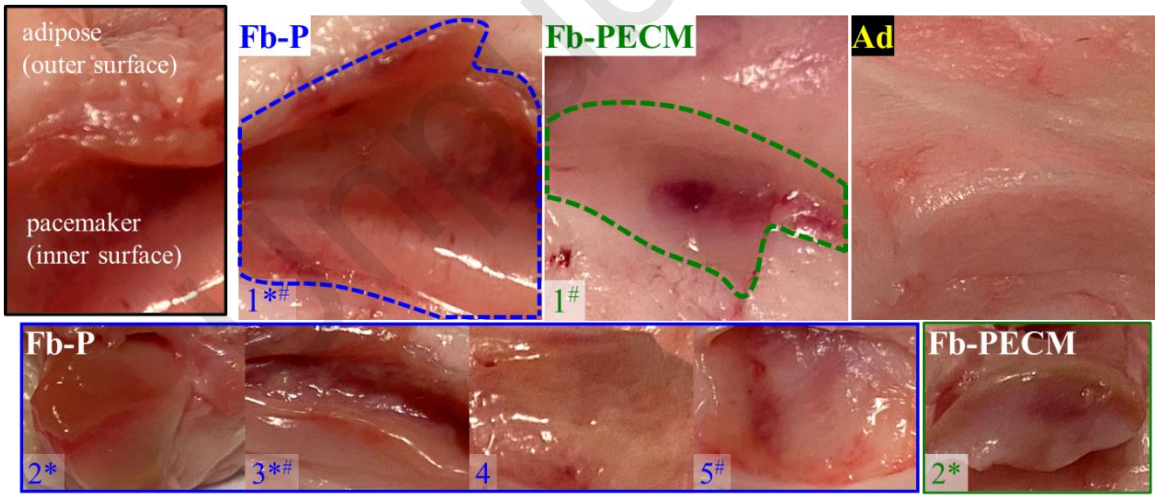

Fig. 3

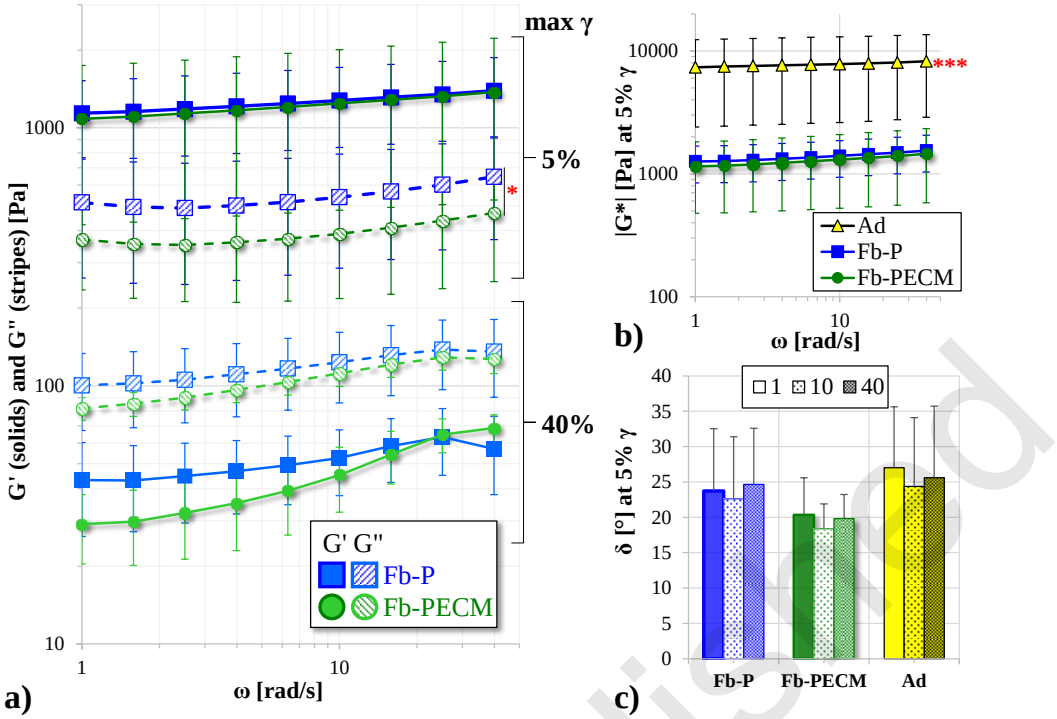

Fig. 4

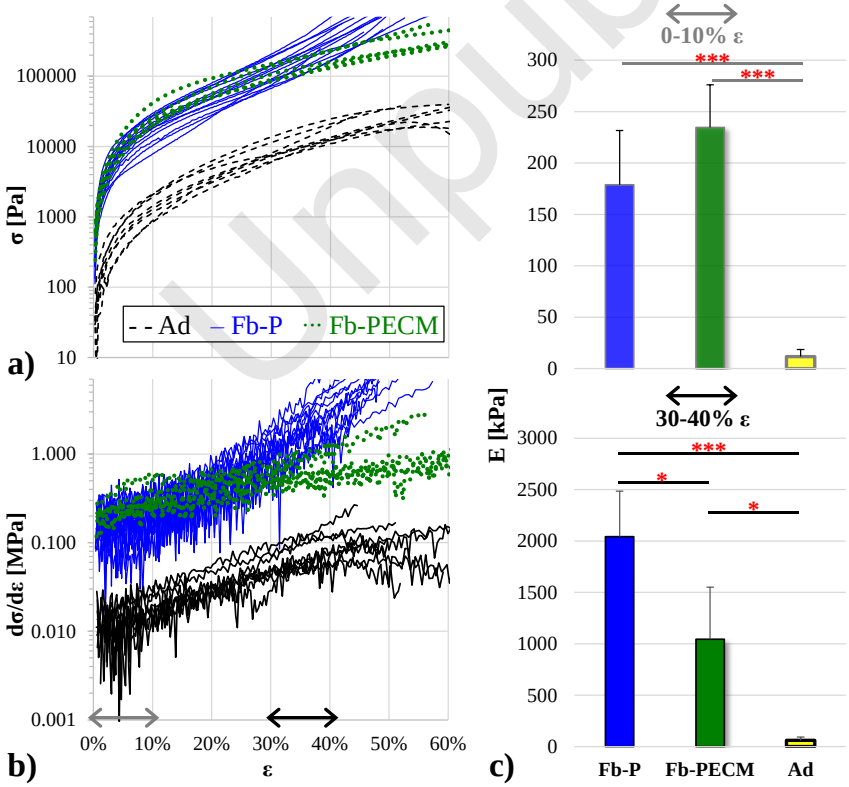

Fig. 5

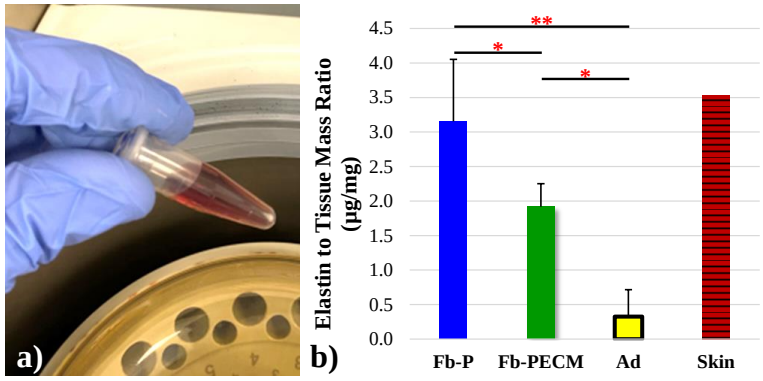

Fig. 6

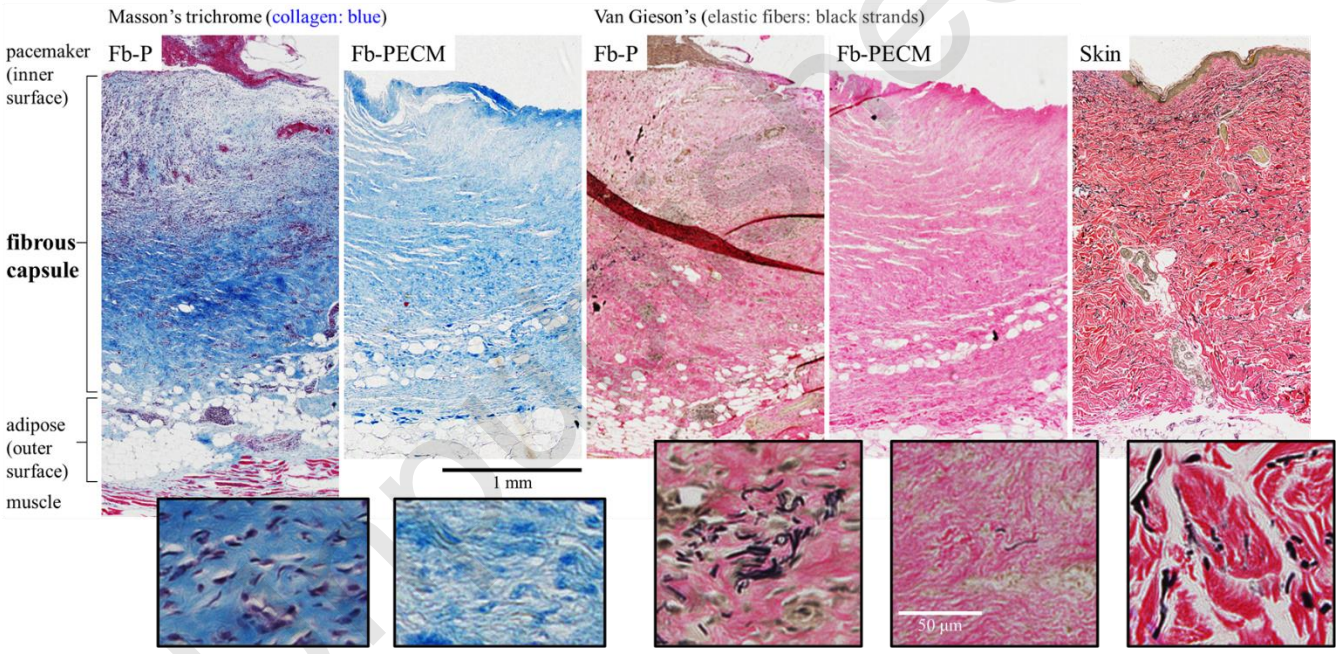

Fig. 7

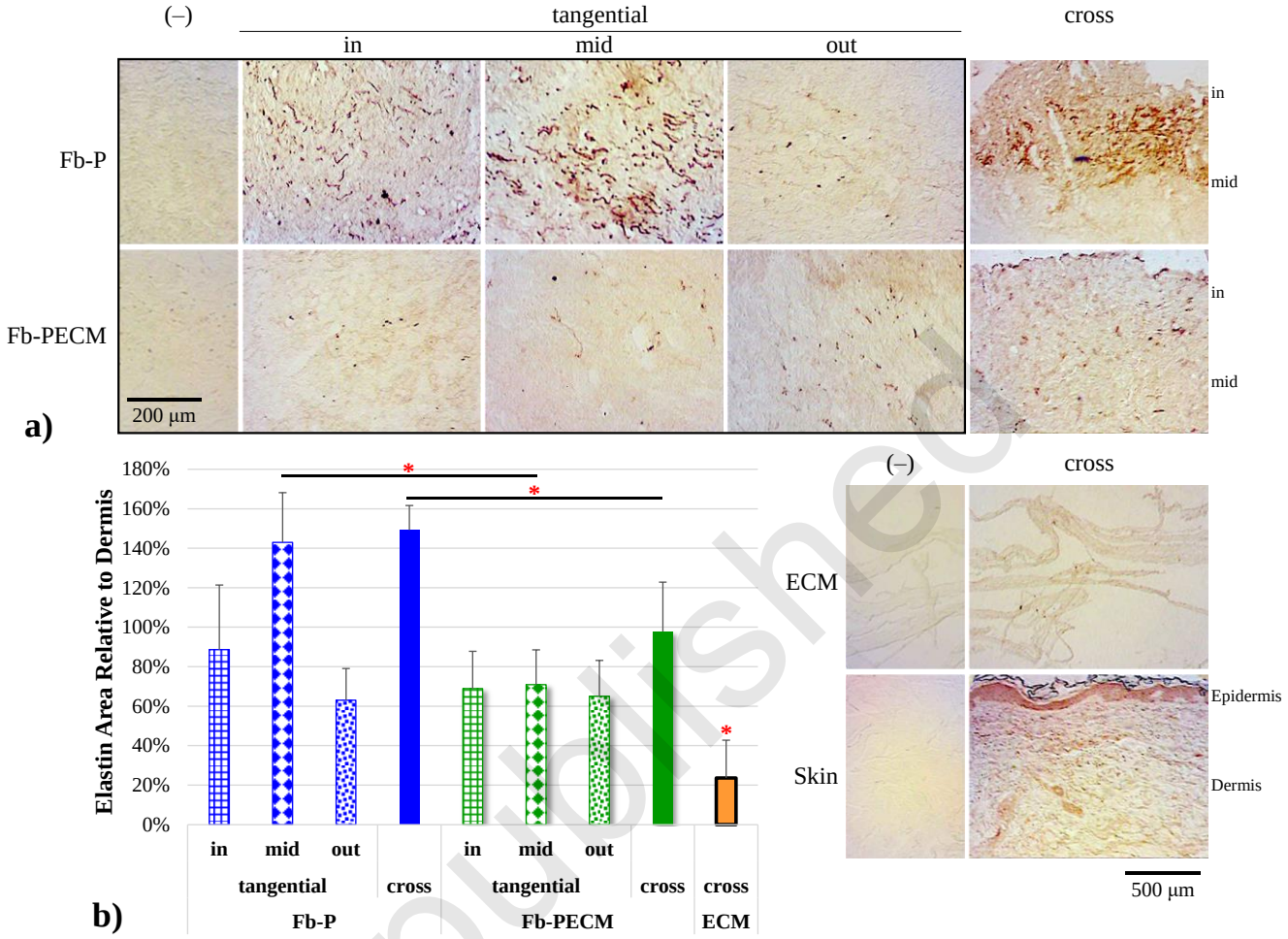

Fig. 8

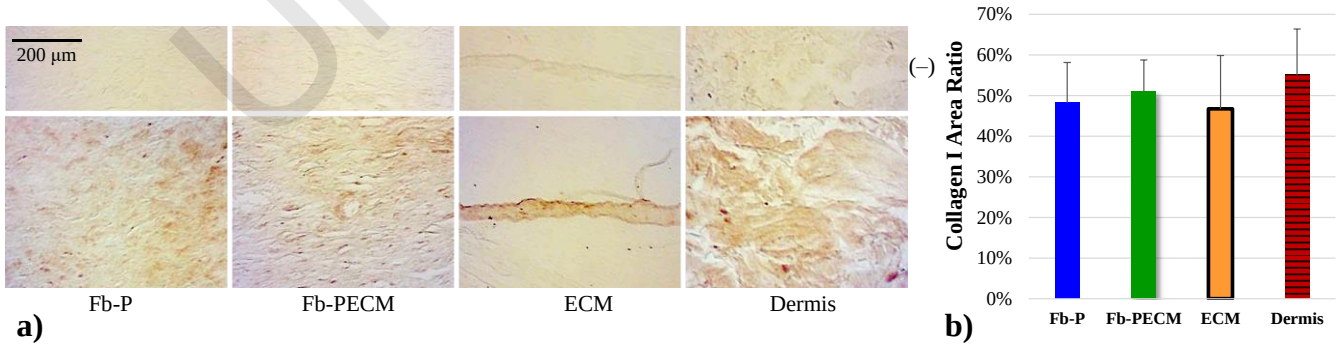

Fig. 9